Received: 22 December 2022 | Accepted: 8 September 2023

DOI: 10.1111/2041-210X.14222

Methods in Ecology and Evolution

RESEARCH ARTICLE

Forecasting wildlife movement with spatial capture–recapture

Nathan J. Crum[1] | Timothy A. Gowan[1] | Kandethody M. Ramachandran[2]

[1]Fish and Wildlife Research Institute, Florida Fish and Wildlife Conservation Commission, St. Petersburg, Florida, USA

[2]Department of Mathematics and Statistics, University of South Florida, Tampa, Florida, USA

Correspondence
Nathan J. Crum
Email: nathan.crum@myfwc.com

Funding information
National Oceanic and Atmospheric Administration, Grant/Award Number: NA16NMF4720319; NOAA Fisheries; US Coast Guard; US Navy; US Army Corps of Engineers; Georgia Department of Natural Resources; Save the Manatee Trust Fund

Handling Editor: Marie Auger-Méthé

Abstract

1. Wildlife movement is an important process affecting species population biology and community interactions in myriad ways. Studies of wildlife movement have focused on retrospectively estimating movements of small numbers of individuals by outfitting them with GPS and telemetry tags. Recent developments in spatial capture–recapture modelling permit the integration of movement models that can estimate the movement of untagged and undetected individuals. Additionally, hidden Markov movement models provide a framework for forecasting individuals' movements, which may be valuable in the conservation of threatened species facing risks that vary across space and time.
2. We describe maximum likelihood estimators for spatial capture–recapture models integrated with simple, biased and correlated random walk movement models formulated as hidden Markov models. Additionally, we demonstrate how to forecast wildlife movement based on these models and hidden Markov model algorithms. We conducted a simulation study to test the performance of the models' abundance estimators and movement forecasts when fit to data simulated under different movement models. We also fit the models to spatial capture–recapture data collected on North Atlantic right whales off the Atlantic Coast of the southeastern United States.
3. Random walk movement models improved abundance estimation and movement forecasts in our simulation study and received greater support from the data in the right whale case study than did activity centre movement models.
4. Forecasts of wildlife movement made under integrated spatial capture–recapture movement models will be most valuable when individuals have been observed recently, when sampling for individuals is extensive and efficient, and when the scale of individuals' movements is small relative to the scale of the study area and sampling process.

KEYWORDS
animal movement, ecological forecasting, *Eubalaena glacialis*, movement ecology, population density, population ecology, right whale, spatial capture–recapture

1 | INTRODUCTION

Wildlife movement is an important process affecting individual space use, migration, encounter rates with predators, prey and anthropogenic threats, population dynamics and gene flow (Matthiopoulos et al., 2015; Morales et al., 2010; Nathan et al., 2008). Therefore, wildlife managers and conservationists often seek to understand wildlife movement to manage habitat features and anthropogenic activities in areas and times where wildlife are expected to be (Runge et al., 2014). Commonly, researchers outfit animals with telemetry or GPS tags to record the animals' movements through time (Cagnacci et al., 2010). However, recent developments in spatial capture–recapture (SCR) allow researchers to model the movement of uniquely identifiable individuals without telemetry or GPS tags (McClintock et al., 2021).

Objectives of individual wildlife movement modelling often include imputing an individual's trajectory (i.e. sequence of locations) between locations collected by GPS tags; estimating movement velocities, turning rates and points or habitat features of attraction and repulsion; and inferring an individual's behavioural state sequence (Hooten et al., 2017). Researchers make inferences on these subjects using hidden Markov models, state space models and diffusion processes (Hooten et al., 2017; Patterson et al., 2017). However, inference is often restricted to a small number of individuals, because costs and logistical constraints limit the number of tagged individuals, that is individuals that are outfitted with GPS or telemetry tags. Additionally, although many studies have focused on predicting the future distribution of wildlife populations (e.g. Hazen et al., 2017), few have focused on forecasting individuals' future movements given their past locations and estimated movement rates (but see Randon et al., 2022). Such forecasts could be useful in further studying the individuals or mitigating threats to them.

The movements of all individuals in a population, not just tagged individuals, may be critically important to understand and forecast, especially in endangered species facing spatially and temporally varying threats. SCR models have been used to estimate wildlife density, habitat selection and space use from data collected from untagged individuals (Royle, Sollman, et al., 2013). Open population SCR models have been used to estimate the movement of individuals' activity centres, that is home range centres (Gardner et al., 2010; Glennie et al., 2019). Bischof et al. (2020) forecasted the annual population size and distribution of wolverines based on the annual activity centre movement, recruitment and mortality rates estimated with an open population SCR model. Additionally, McClintock et al. (2021) proposed a framework for integrating random walk (RW) movement models with SCR. These integrated SCR movement models have been implemented primarily in Bayesian frameworks. For instance, Gardner et al. (2022) simulated data from and fit SCR models integrated with correlated RW and Langevin movement models; Hostetter et al. (2022) estimated polar bear density and movement with SCR models integrated with simple and correlated RWs; and Chandler et al. (2021) estimated white-tailed deer density and movement with SCR models integrated with biased RWs. Integrated SCR movement models could also allow researchers to forecast the movements of individuals.

We describe a SCR model integrated with hidden Markov models for simple, biased and correlated RWs using a maximum likelihood estimation framework. Our model differs from other maximum likelihood-based SCR models (Efford & Schofield, 2020; Glennie et al., 2019) by modelling the movement of individuals rather than their activity centres and by permitting bias and correlation in movement direction and speed. As with the conventional activity centre model used in SCR analyses, the biased RW accounts for the bias of an individual's movement toward a point of attraction, an important property of some species' movement behaviours. Each RW exhibits another important property of animal movement: serial correlation of an individual's locations. Additionally, the correlated RW exhibits serial correlation of an individual's speed and direction. We show through a simulation study that these models can be fit to relatively sparse data characteristic of SCR studies. We also evaluate model performance in estimating abundance and forecasting movements of individuals. Finally, we estimate North Atlantic right whale (*Eubalaena glacialis*) population size, population dynamics and movement in the coastal waters of the southeastern United States using integrated SCR movement models.

2 | METHODS

2.1 | Model formulation

Consider a study region, $\boldsymbol{S}$, containing an unknown number of individuals, N. Let $\boldsymbol{S}$ be partitioned into m subregions. SCR sampling is conducted over T occasions, during which n individuals are detected at least once, and $n \leq N$. Sampling may be conducted using a fixed array of detectors or through search-encounter surveys. Individuals must be uniquely marked during their first detection or be identifiable through natural markings. The encounter history for individual i, $\boldsymbol{y}_i$, is a vector of length T, where $\boldsymbol{y}_{i,t} = 1$ if individual i was detected on occasion t, and $\boldsymbol{y}_{i,t} = 0$ otherwise. When individual i is detected on occasion t, the subregion in which it is located, $\boldsymbol{u}_{i,t}$, and auxiliary data such as the distance between the individual and detector making the detection, $\boldsymbol{d}_{i,t}$, are recorded. Here, we assume that individuals can be detected at most once during an occasion, although see Hostetter et al. (2022) for an approach to relax this assumption.

We formulate a SCR model using a hidden Markov model to account for the partially observed movement trajectories of individuals through subregions of $\boldsymbol{S}$ and a thinned Poisson point process describing the number of individuals observed at least once. The hidden Markov model contains three components: the initial state distribution, $\boldsymbol{\delta}$, the state transition matrix, $\boldsymbol{\Gamma}$, and the state-dependent detection process, $\boldsymbol{P}(\boldsymbol{y}_{i,t}, \boldsymbol{u}_{i,t}, \boldsymbol{d}_{i,t})$. In this context, an individual's state may correspond to the subregion in $\boldsymbol{S}$ in which it is located or to some combination of its current subregion, past subregions and

activity centre. In a model where states have one-to-one correspondence with subregions, $\boldsymbol{\delta}$ is a row vector of length m, and $\boldsymbol{\delta}_j$ is the probability that an individual is in state j, that is subregion j, on the first sampling occasion. Then, $\boldsymbol{\Gamma}$ is an $m \times m$ matrix whose element in the j-th row, k-th column, $\boldsymbol{\Gamma}_{j,k}$, is the probability that an individual in state j at time t will be in state k at time $t+1$. Finally, $\boldsymbol{P}(\boldsymbol{y}_{i,t}, \boldsymbol{u}_{i,t}, \boldsymbol{d}_{i,t})$ is an $m \times m$ diagonal matrix whose j-th diagonal element is the probability of observing $\boldsymbol{y}_{i,t}$, $\boldsymbol{u}_{i,t}$ and $\boldsymbol{d}_{i,t}$ given that individual i is in state j at time t. The likelihood of individual i's encounter history under the hidden Markov model is:

$$L_i = \boldsymbol{\delta}\left(\prod_{t=1}^{T-1} \boldsymbol{P}(\boldsymbol{y}_{i,t}, \boldsymbol{u}_{i,t}, \boldsymbol{d}_{i,t})\boldsymbol{\Gamma}\right)\boldsymbol{P}(\boldsymbol{y}_{i,T}, \boldsymbol{u}_{i,T}, \boldsymbol{d}_{i,T})\boldsymbol{\varepsilon} \quad (1)$$

where $\boldsymbol{\varepsilon}$ is a column vector of ones of length m.

In all models described hereafter, the state-dependent detection process, $\boldsymbol{P}(\boldsymbol{y}_{i,t}, \boldsymbol{u}_{i,t}, \boldsymbol{d}_{i,t})$, constrains the probability of detecting an individual in a subregion in which it is not located to 0, that is the model assumes false-positive detections cannot occur. Therefore, when $\boldsymbol{y}_{i,t}=1$ and $\boldsymbol{u}_{i,t}=j$, only the j-th diagonal element of $\boldsymbol{P}(\boldsymbol{y}_{i,t}, \boldsymbol{u}_{i,t}, \boldsymbol{d}_{i,t})$ is non-zero. In studies where $\boldsymbol{d}$ is collected, the j-th diagonal element of $\boldsymbol{P}(\boldsymbol{y}_{i,t}, \boldsymbol{u}_{i,t}, \boldsymbol{d}_{i,t})$ is $g(\boldsymbol{d}_{i,t})$, a decreasing function of $\boldsymbol{d}_{i,t}$, as in distance sampling (Buckland et al., 2004). For instance, the half-normal, $\boldsymbol{P}(\boldsymbol{y}_{i,t}, \boldsymbol{u}_{i,t}, \boldsymbol{d}_{i,t})_{jj} = g(\boldsymbol{d}_{i,t}) = g0\exp\left(-\frac{d_{i,t}^2}{2\sigma_d^2}\right)$, or hazard-rate, $\boldsymbol{P}(\boldsymbol{y}_{i,t}, \boldsymbol{u}_{i,t}, \boldsymbol{d}_{i,t})_{jj} = g(\boldsymbol{d}_{i,t}) = g0\exp\left(-\left(\frac{d_{i,t}}{\sigma_d}\right)^{-\beta_d}\right)$, functions may be used, where $g0$ is the probability of detecting an individual located at 0 distance from a detector, and σ_d and β_d describe the decay function of detection probability. When $\boldsymbol{d}$ is not relevant, the j-th diagonal element of $\boldsymbol{P}(\boldsymbol{y}_{i,t}, \boldsymbol{u}_{i,t}, \boldsymbol{d}_{i,t})$ may be some constant, state-varying, time-varying or effort-varying detection probability. When $\boldsymbol{y}_{i,t}=0$, $\boldsymbol{P}(\boldsymbol{y}_{i,t}, \boldsymbol{u}_{i,t}, \boldsymbol{d}_{i,t})$ holds the probabilities of an individual not being detected given it is in each state. These values are one minus the detection probability for each state when $\boldsymbol{d}$ is not relevant. When $\boldsymbol{d}$ is relevant to the detection process, the probability of an individual in state j not being detected is $1 - \frac{1}{|\boldsymbol{s}_j|}\int_{\boldsymbol{s}_j} g(d)d\boldsymbol{s}_j$, where $\boldsymbol{s}_j$ is the j-th subregion of $\boldsymbol{S}$ and d is the distance from each point in $\boldsymbol{s}_j$ to the location of the nearest detector (Crum et al., 2021; Gowan et al., 2021). This formulation assumes that the location of an individual within $\boldsymbol{s}_j$ is distributed uniformly. When different points in $\boldsymbol{s}_j$ are nearest different detectors, the detection function must be integrated over subregions of $\boldsymbol{s}_j$. When $\boldsymbol{s}_j$ must be partitioned into l subregions, the probability that an individual in state j is not detected is $1 - \frac{1}{|\boldsymbol{s}_j|}\sum_{k=1}^{l}\int_{\boldsymbol{s}_{j,k}} g(d)d\boldsymbol{s}_{j,k}$, where $\boldsymbol{s}_{j,k}$ is the k-th subregion of $\boldsymbol{s}_j$. Partitioning $\boldsymbol{s}_j$ for only the detection process, rather than both the detection and state transition processes, can significantly reduce the computation required for the model. In application, we use numerical integration to calculate the probabilities that an individual is not detected given its state.

In a simple RW movement model, the states of the hidden Markov model have one-to-one correspondence with subregions in $\boldsymbol{S}$, meaning the model will have m states. In such a model, $\boldsymbol{\delta}$ may be uniformly distributed, $\boldsymbol{\delta} = \left(\frac{1}{m}, \frac{1}{m}, \ldots \frac{1}{m}\right)$, or distributed according to some spatially explicit environmental covariates, $\boldsymbol{Z}$, $\boldsymbol{\delta} = \left(\frac{\exp(\boldsymbol{Z}_1\boldsymbol{\beta})}{\sum_{j=1}^{m}\exp(\boldsymbol{Z}_j\boldsymbol{\beta})}, \frac{\exp(\boldsymbol{Z}_2\boldsymbol{\beta})}{\sum_{j=1}^{m}\exp(\boldsymbol{Z}_j\boldsymbol{\beta})}, \ldots, \frac{\exp(\boldsymbol{Z}_m\boldsymbol{\beta})}{\sum_{j=1}^{m}\exp(\boldsymbol{Z}_j\boldsymbol{\beta})}\right)$. Here, $\boldsymbol{Z}$ is a matrix with m rows, corresponding to the m subregions, and with one column for each covariate, and $\boldsymbol{\beta}$ is a vector with length equal to the number of covariates. State transition probabilities are a function of the distance between the centres of subregions and may be a function of environmental covariates, for example $\boldsymbol{\Gamma}_{j,k} = \frac{f(d_{\text{move},j,k}, \boldsymbol{Z}_k\boldsymbol{\beta})}{\sum_{l=1}^{m} f(d_{\text{move},j,l}, \boldsymbol{Z}_l\boldsymbol{\beta})}$, where $d_{\text{move},j,k}$ is the distance between the centres of $\boldsymbol{s}_j$ and $\boldsymbol{s}_k$, and f is a function of this distance. For instance, f may approximate the exponential distribution, $f\left(d_{\text{move},j,k}, \boldsymbol{Z}_k\boldsymbol{\beta}\right) = \exp\left(-\frac{d_{\text{move},j,k}}{\sigma_{\text{move}}} + \boldsymbol{Z}_k\boldsymbol{\beta}\right)$, where σ_{move} describes the scale of an individual's movement. We share $\boldsymbol{\beta}$ across $\boldsymbol{\delta}$ and $\boldsymbol{\Gamma}$ for model simplicity, but different sets of parameters could be used in practice. Additionally, we measure d_{move} with Euclidean distance, but the model could be modified to use least-cost distances (Dupont et al., 2021; Royle, Chandler, Gazenski, et al., 2013).

In a biased RW movement model, an individual's state describes the subregion in which it is located and the subregion in which the activity centre or source of bias is located. Therefore, such a hidden Markov model will have m^2 states. We formulate $\boldsymbol{\delta}$ such that an activity centre is distributed equivalently to the initial location in the simple RW described above. Then, given an activity centre is located in $\boldsymbol{s}_j$, the initial subregion in which the individual is located is distributed following the j-th row of $\boldsymbol{\Gamma}$ as described in the simple RW model. Assuming that an individual's activity centre remains constant over the course of sampling, $\boldsymbol{\Gamma}$ is a $m^2 \times m^2$ block diagonal matrix. Block matrices of $\boldsymbol{\Gamma}$ are of dimension $m \times m$, and the j-th block describes the transition probabilities among subregions of $\boldsymbol{S}$ given an individual has an activity centre in $\boldsymbol{s}_j$. Elements of each block matrix are identical to those of $\boldsymbol{\Gamma}$ under the simple RW. However, for block j, $d_{\text{move},k,l}$ is the distance from the centre of $\boldsymbol{s}_l$, the individual's location at time $t+1$, to the weighted average of the centres of $\boldsymbol{s}_k$ and $\boldsymbol{s}_j$, the individual's location at time t and activity centre, respectively, $\sqrt{(x_l - \rho x_k - (1-\rho)x_j)^2 + (y_l - \rho y_k - (1-\rho)y_j)^2}$, where (x_j, y_j) is the centre point of $\boldsymbol{s}_j$. Here, ρ is a parameter bounded between zero and one that describes the strength of bias toward the activity centre. When ρ is one, the biased RW simplifies to the simple RW, and when ρ is zero, the biased RW simplifies to a static activity centre model, where an individual's location at time $t+1$ depends only on the location of its activity centre.

In a correlated RW movement model, an individual's state describes both the current and previous subregions in which it has been located. In the case of a second-order correlated RW, a hidden Markov model will have m^2 states. We formulate $\boldsymbol{\delta}$ identically to our formulation in the biased RW, except here, instead of an individual's activity centre being uniformly distributed, its location prior to its initial location is uniformly distributed. Elements of $\boldsymbol{\Gamma}$ are formulated in the same way as in the simple RW model. However, $d_{\text{move},j,k,l}$ is the distance from the centre of $\boldsymbol{s}_l$, the individual's location at time $t+1$, to the expected trajectory of movement for an individual in $\boldsymbol{s}_k$ at time t, having travelled from $\boldsymbol{s}_j$ at time $t-1$, $\sqrt{(x_l - x_k - \gamma(\cos(\omega) * (x_k - x_j) - \sin(\omega) * (y_k - y_j)))^2 + (y_l - y_k - \gamma(\sin(\omega) * (x_k - x_j) + \cos(\omega) * (y_k - y_j)))^2}$. Here, γ, bounded by 0 and 1, and ω, bounded by $-\pi$ and π, are parameters describing the correlation in the movement length and direction across time. Additionally, $\boldsymbol{\Gamma}$ is a sparse matrix because only

an individual in a state corresponding to being in s_k at time t can transition to a state corresponding to being in s_k at time $t-1$.

In this SCR model, the hidden Markov model describes processes for the movement and detection of individuals in the population of interest, and a Poisson point process describes the number of individuals in the population, that is abundance, and their expected distribution at the beginning of the time series, $\left(\exp(\beta_0+\boldsymbol{Z}_1\boldsymbol{\beta}),\exp(\beta_0+\boldsymbol{Z}_2\boldsymbol{\beta}),\ \ldots\ ,\exp(\beta_0+\boldsymbol{Z}_m\boldsymbol{\beta})\right)$, where β_0 is an intercept effect. Following Borchers and Efford (2008) and Glennie et al. (2019), we formulate the model likelihood conditional on n individuals being observed at least once. The probability of an individual being observed at least once, p^*, is $1-\boldsymbol{\delta}\left(\prod_{t=1}^{T-1}\boldsymbol{P}(\boldsymbol{y}_{i,t}=0)\boldsymbol{\Gamma}\right)\boldsymbol{P}(\boldsymbol{y}_{i,T}=0)\boldsymbol{\varepsilon}$. The likelihood of n individuals being observed at least once under the Poisson point process is $\frac{(Dp^*)^n\exp(-Dp^*)}{n!}$, where D is the expected population abundance, that is the parameter that estimates N. The full model likelihood follows as:

$$L=\frac{(Dp^*)^n\exp(-Dp^*)}{n!}*\prod_{i=1}^{n}\frac{1}{p^*}*\boldsymbol{\delta}\left(\prod_{t=1}^{T-1}\boldsymbol{P}(\boldsymbol{y}_{i,t},\boldsymbol{u}_{i,t},\boldsymbol{d}_{i,t})\boldsymbol{\Gamma}\right)\boldsymbol{P}(\boldsymbol{y}_{i,T},\boldsymbol{u}_{i,T},\boldsymbol{d}_{i,T})\boldsymbol{\varepsilon} \tag{2}$$

We wrote likelihood functions in R and C++ using the Rcpp package and use numerical optimization for maximum likelihood estimation (Eddelbuettel & Francois, 2011; Eddelbuettel & Sanderson, 2014; R Core Team, 2019).

2.2 | Density and movement estimation

The location of an individual during an occasion can be estimated using the forward–backward algorithm (Zucchini et al., 2016). Let $\boldsymbol{\alpha}_{i,t}$ be the forward probabilities, and $\boldsymbol{\gamma}_{i,t}$ be the backward probabilities for individual i on occasion t where

$$\boldsymbol{\alpha}_{i,t}=\boldsymbol{\delta}\left(\prod_{v=1}^{t-1}\boldsymbol{P}(\boldsymbol{y}_{i,v},\boldsymbol{u}_{i,v},\boldsymbol{d}_{i,v})\boldsymbol{\Gamma}\right)\boldsymbol{P}(\boldsymbol{y}_{i,t},\boldsymbol{u}_{i,t},\boldsymbol{d}_{i,t})$$

$$\boldsymbol{\gamma}'_{i,t}=\left(\prod_{v=t+1}^{T}\boldsymbol{\Gamma}\boldsymbol{P}(\boldsymbol{y}_{i,v},\boldsymbol{u}_{i,v},\boldsymbol{d}_{i,v})\right)\boldsymbol{\varepsilon}' \tag{3}$$

Here, $\boldsymbol{\alpha}_{i,t}$ and $\boldsymbol{\gamma}_{i,t}$ are vectors of length m, and the j-th elements are the relative probabilities that individual i is located in s_j on occasion t given individual i's encounter history before and including occasion t and its encounter history after occasion t, respectively. The dot product of $\boldsymbol{\alpha}_{i,t}$ and $\boldsymbol{\gamma}_{i,t}$ is the likelihood of individual i's encounter history, L_i. The distribution of the individual's location given its entire encounter history is the elementwise product of $\boldsymbol{\alpha}_{i,t}$ and $\boldsymbol{\gamma}_{i,t}$ scaled to sum to one, $\frac{(\boldsymbol{\alpha}_{i,t}\circ\boldsymbol{\gamma}_{i,t})}{L_i}$. It follows that the realized population density on occasion t is $\sum_{i=1}^{n}\frac{(\boldsymbol{\alpha}_{i,t}\circ\boldsymbol{\gamma}_{i,t})}{L_i}+D(1-p^*)\frac{(\boldsymbol{\alpha}_{n+1,t}\circ\boldsymbol{\gamma}_{n+1,t})}{L_{n+1}}$ and the average realized population density over all sampling occasions is $\frac{1}{T}\sum_{t=1}^{T}\left(\sum_{i=1}^{n}\left(\frac{(\boldsymbol{\alpha}_{i,t}\circ\boldsymbol{\gamma}_{i,t})}{L_i}\right)+D(1-p^*)\frac{(\boldsymbol{\alpha}_{n+1,t}\circ\boldsymbol{\gamma}_{n+1,t})}{L_{n+1}}\right)$, where $\boldsymbol{\alpha}_{n+1,t}$ and $\boldsymbol{\gamma}_{n+1,t}$ are the forward and backward probabilities for an individual that was never observed. Additionally, L_{n+1} is the likelihood of an individual that was never observed, $\boldsymbol{\delta}\left(\prod_{t=1}^{T-1}\boldsymbol{P}(\boldsymbol{y}_{i,t}=0)\boldsymbol{\Gamma}\right)\boldsymbol{P}(\boldsymbol{y}_{i,T}=0)\boldsymbol{\varepsilon}$. The expected population density, which does not explicitly account for individuals' encounter histories, on occasion t is the product of expected abundance, the initial state vector and $t-1$ state transition matrices, $D\boldsymbol{\delta}\boldsymbol{\Gamma}^{t-1}$. The average expected density over all sampling occasions is $\frac{1}{T}\sum_{t=1}^{T}D\boldsymbol{\delta}\boldsymbol{\Gamma}^{t-1}$. Each expression of density results in a vector whose j-th element is the estimated number of individuals in state j over the time period of interest.

2.3 | Hidden Markov model forecasting

Given the observed data and estimated parameters from the model described above, individuals' future locations can be forecast. The first step in forecasting locations is to estimate an individual's location at time T, the last sampling occasion. Here, we use the forward–backward algorithm to estimate the distribution of the location of individual i, which was observed at least once over the previous T occasions (Zucchini et al., 2016). At time T, $\boldsymbol{\gamma}_{i,T}$ is $\boldsymbol{\varepsilon}$, therefore this distribution is $\boldsymbol{\alpha}_{i,T}$ scaled to sum to one, $\frac{\boldsymbol{\delta}\left(\prod_{t=1}^{T-1}\boldsymbol{P}(\boldsymbol{y}_{i,t},\boldsymbol{u}_{i,t},\boldsymbol{d}_{i,t})\boldsymbol{\Gamma}\right)\boldsymbol{P}(\boldsymbol{y}_{i,T},\boldsymbol{u}_{i,T},\boldsymbol{d}_{i,T})}{L_i}$. Then, on sampling occasion $T+h$, the distribution of the individual's state given the observed data from sampling occasions 1 to T is $\frac{\boldsymbol{\alpha}_{i,T}\boldsymbol{\Gamma}^h}{L_i}$, whose j-th element is the probability that the individual will be in s_j. Additionally, there are an estimated $D(1-p^*)$ individuals that were unobserved on occasions 1 to T. The locations of these individuals can be forecast collectively. On occasion T, they are distributed according to a Poisson point process with intensity $\frac{D(1-p^*)\boldsymbol{\alpha}_{n+1,T}}{L_{n+1}}$. Then, on sampling occasion $T+h$, the forecasted distribution of the $N-n$ individuals is $\frac{D(1-p^*)\boldsymbol{\alpha}_{n+1,T}\boldsymbol{\Gamma}^h}{L_{n+1}}$. The joint likelihood of all individuals' locations under the forecast on occasion $T+h$ is $\left(\prod_{i=1}^{n}\frac{\boldsymbol{\alpha}_{i,T}\boldsymbol{\Gamma}^h\boldsymbol{P}(\boldsymbol{u}_{i,T+h})}{L_i}\right)\left(\frac{(D(1-p^*))^{N-n}\exp(-D(1-p^*))}{(N-n)!}\prod_{i=n+1}^{N}\frac{\boldsymbol{\alpha}_{n+1,T}\boldsymbol{\Gamma}^h\boldsymbol{P}(\boldsymbol{u}_{i,T+h})}{L_{n+1}}\right)$, where the j-th diagonal element of $\boldsymbol{P}(\boldsymbol{u}_{i,T+h})$ is a one when individual i was located in s_j on occasion $T+h$, and all other elements are zero. Additionally, the joint likelihood of all individuals' encounter histories on occasion $T+h$ is $\left(\prod_{i=1}^{n}\frac{\boldsymbol{\alpha}_{i,T}\boldsymbol{\Gamma}^h\boldsymbol{P}(\boldsymbol{y}_{i,T+h},\boldsymbol{u}_{i,T+h},\boldsymbol{d}_{i,T+h})}{L_i}\right)\left(\frac{(D(1-p^*))^q\exp\left(-D(1-p^*)p^*_{T+h}\right)}{q!}\prod_{i=n+1}^{n+q}\frac{\boldsymbol{\alpha}_{n+1,T}\boldsymbol{\Gamma}^h\boldsymbol{P}(\boldsymbol{y}_{i,T+h},\boldsymbol{u}_{i,T+h},\boldsymbol{d}_{i,T+h})}{L_{n+1}}\right)$, where q individuals were observed on occasion $T+h$ that had not been observed on or before occasion T, and p^*_{T+h} is the probability of detecting an individual on occasion $T+h$ that had not been observed on or before occasion T.

2.4 | Simulation study

We simulated 1000 closed population SCR data sets under three scenarios. In the first scenario, individuals moved according to a simple RW; in the second, individuals moved according to a biased RW; and in the third, individuals moved according to a correlated RW. In each scenario, a population of 100 individuals was simulated with a uniform initial density. The study region, $\boldsymbol{S}$, was square, 1600 unit^2, and divided into 1600 one unit^2 subregions. We simulated individuals' movements across subregions following the exponential distribution, that is $f(d_{\text{move},j,k})=\exp\left(-\frac{d_{\text{move},j,k}}{\sigma_{\text{move}}}\right)$. Individuals' locations were uniformly distributed within the subregions in which they

were located. Data were simulated over 20 sampling occasions. On each sampling occasion, individuals were subject to sampling from 10 parallel line transects that were 20 units long and had two-unit spacing. The probability of an individual being detected was a half-normal function of its distance to the closest transect. We provide additional simulation details in Appendix 1. For each scenario, we fit SCR models to data from the first 10 sampling occasions. We divided $\boldsymbol{S}$ into 400 four-unit^2 subregions for models fit to simulated data, which decreased the computation required for each model, especially the biased and correlated RW models. We estimated realized abundance, that is the sum of realized density across $\boldsymbol{S}$, (Efford & Fewster, 2013) and calculated the likelihood of individuals' locations and encounter histories over the next 10 sampling occasions under forecasts from each model. Additionally, we evaluated the calibration of forecasts from each model, that is we calculated the proportions of locations falling within forecasted confidence regions of varying confidence levels. This approach is analogous to using pseudo or quantile residuals to test for goodness of fit (Dunn & Smyth, 1996; Zucchini et al., 2016). For the first scenario, we fit SCR models with static activity centre, that is a biased RW with ρ fixed to zero, and simple RW movement models. For the second scenario, we fit models with static activity centre, simple and biased RW movement models. For the third scenario we fit models with static activity centre, simple and correlated RW movement models. In all scenarios, we fit models with exponentially distributed movement, matching the distribution for simulated movement. We provide an R package, scrrw, with functions to simulate encounter histories, fit SCR movement models and forecast individuals' movements.

2.5 | North Atlantic right whale abundance and movement

The North Atlantic right whale is an endangered large whale species that inhabits the coastal waters of the eastern United States and Canada. Some right whales migrate to the coastal waters of the southeastern United States, hereafter referred to as the Southeast, each winter (Gowan et al., 2019; Krzystan et al., 2018). Throughout their range, right whales are at risk of being struck and killed or severely injured by vessels; therefore, understanding and predicting their movements could provide valuable information to managers working to mitigate the threat of vessel strikes (Crum et al., 2019; van der Hoop et al., 2014). We fit open SCR models to right whale encounter history data collected from aerial surveys off the Southeast between 1 December 2009 and 31 March 2010 (see Gowan et al., 2021; Gowan & Ortega-Ortiz, 2014 for detailed descriptions of data collection). We divided our study region (Appendix 2 in Figure S1) into 772 100 km^2 sub-regions for the model. We augmented the models described in the model formulation section with two additional unobservable states, one for individuals that had yet to immigrate to the Southeast and another for individuals that had already emigrated from the Southeast or had died, although we expect deaths were rare as right whale annual survival exceeds 0.95 (Pace et al., 2017). The probability that an individual not in the Southeast immigrated to the Southeast, τ, was modelled as a quadratic function of t, the number of days since 1 December, $\tau_t = \frac{1}{1+\exp(-(\beta_0+\beta_1*t+\beta_2*t^2))}$. The probability that an individual in the Southeast remained in the Southeast, φ, was modelled as a linear function of the number of days since 1 December, $\varphi_t = \frac{1}{1+\exp(-(\beta_3+\beta_4*t))}$. The model permitted migration during one state transition every 10 days, and the population was closed on all other transitions. We modelled daily movement according to activity centre, simple and correlated RW movement models where movement was an exponentially declining function of distance. In the activity centre model, individuals' activity centres could move every 10 days and were independent of past activity centres. We simplified the correlated RW model to shorten computation time by accounting only for correlation in movement direction and classifying movements into four categories, north, south, east and west. For each movement model, we tested a null model without environmental covariates and a model that included quadratic effects of depth and sea surface temperature and a linear effect of wind speed, $f(d_{\text{move},j,k}, \boldsymbol{Z}_k\boldsymbol{\beta}) = \exp\left(-\frac{d_{\text{move},j,k}}{\sigma_{\text{move}}} + \beta_5*\text{sst}_k + \beta_6*\text{sst}_k^2 + \beta_7*\text{depth}_k + \beta_8*\text{depth}_k^2 + \beta_9*ws_k\right)$. We fit models to the full dataset and used AIC for model comparison (Burnham & Anderson, 2002). Additionally, we fit models to a reduced dataset, which omitted every 10th sampling occasion starting with the seventh occasion, that is the seventh, 17th, 27th, etc. To evaluate the forecasting skill of each model, we generated forecasts for the locations of all individuals, previously observed and unobserved, on the omitted occasions based on the models' parameter estimates and the data collected preceding each omitted occasion. We compared models' forecast skill by comparing the likelihood of omitted data under forecasts from each model.

3 | RESULTS

3.1 | Simulation study

SCR models estimated abundance with relative bias ≤5% in most cases, regardless of movement model specification (Table 1). Mean square error of abundance estimates was the smallest in cases where the specified movement model matched the model used to simulate the data (Table 1). Models that matched the simulating model also predicted future locations of individuals with the highest likelihood, and their forecasts were well calibrated, that is the confidence level of forecast regions matched the proportion of locations that fell within them (Figure 1).

When individuals' movements were simulated according to a simple RW, forecasts from the activity centre model became less likely relative to the simple RW forecasts as time since the last sampling occasion increased (Appendix 1 in Figure S3). Additionally, forecast regions generated by the activity centre model contained fewer locations of individuals than expected and this miscalibration worsened over time (Appendix 1 in Figure S4).

When individuals' movements were simulated according to a biased RW, the likelihoods of the activity centre and simple RW

TABLE 1 Properties of spatial capture–recapture abundance estimates. One thousand data sets each were simulated with 100 individuals following a simple random walk, biased random walk or correlated random walk movement model. Spatial capture–recapture models with activity centre, simple random walk, biased random walk and correlated random walk movement models were fit to the simulated datasets to estimate realized abundance. We calculated bias (the average difference between estimated and true abundance), confidence interval coverage (the proportion of estimated confidence intervals containing the true value of abundance), confidence interval size (the average width of abundance confidence intervals) and mean square error (the average squared difference between estimated and true abundance).

Simulating movement model	Fitted movement model	Bias	Confidence interval coverage	Confidence interval size	MSE
Simple random walk	Activity centre	11.38	0.898	103.48	836.20
	Simple random walk	2.56	0.953	92.54	511.66
Biased random walk	Activity centre	3.83	0.942	89.10	504.24
	Simple random walk	−4.47	0.927	82.92	531.24
	Biased random walk	1.80	0.942	88.91	499.02
Correlated random walk	Activity centre	4.82	0.930	85.60	504.65
	Simple random walk	1.26	0.951	81.48	402.57
	Correlated random walk	2.54	0.944	79.75	390.65

forecasts were similar and lower than the likelihood of the biased RW forecast on the first forecasted occasion. Following the first forecasted occasion, the likelihoods of the activity centre forecasts remained the same across time relative to the biased RW forecasts, whereas the likelihoods of the simple RW forecasts decreased over time relative to the biased RW forecasts (Appendix 1 in Figure S7). Forecasted regions generated by the activity centre model contained fewer locations of individuals than expected, while those generated by the simple RW model contained more locations than expected. This miscalibration increased with time (Appendix 1 in Figure S8).

When individuals' movements were simulated according to a correlated RW, the likelihoods of the activity centre forecasts decreased sharply over time relative to the correlated RW forecasts, while the likelihoods of the simple RW forecasts decreased over the first few occasions and then plateaued relative to the correlated RW forecasts (Appendix 1 in Figure S11). Forecast regions generated by the activity centre and simple RW models contained fewer locations of individuals than expected. This miscalibration was worse in the activity centre model and worsened with time under both models (Appendix 1 in Figure S12).

3.2 | North Atlantic right whale abundance and movement

Aerial surveys were conducted on 77 days between 1 December 2009 and 31 March 2010 and observed 214 individual right whales at least once. Individuals were observed an average of 4.1 times (range: 1–17). Abundance estimates were smallest for models with an activity centre movement model and largest for models with a simplified correlated RW movement model (Table 2). The correlated RW movement model received the most support in the data followed by the simple RW and then the activity centre movement model (Table 2). However, data omitted from the reduced data set were more likely under forecasts generated by the simple RW than under the correlated RW (Table 2). The correlated and simple RW models estimated that right whales moved 26–35 km per day on average (Table 2). Models that included the effects of environmental covariates on movement received considerably greater support in the data and generated better forecasts than models without environmental covariates (Figure 2). These models all estimated that right whales moved to areas of lower wind speeds and depths around 20 m (Appendix 2 in Figure S2). The simple RW and activity centre models estimated that right whales moved to areas with sea surface temperatures around 14°C, while the correlated RW model produced unreasonable estimates of the association between right whale movements and sea surface temperature (Appendix 2 in Figure S2).

4 | DISCUSSION

We describe a maximum likelihood estimator for a SCR model integrated with RW movement models and a framework to forecast future locations of wildlife. Our simulation study and right whale case study demonstrate the value of using more realistic and complex movement models than static activity centre models. Incorporating complex space use or movement models into SCR can reduce bias in abundance estimates (Chandler et al., 2021; Royle, Chandler, Sun, et al., 2013). Likewise, the RW movement models improved estimation of abundance and forecast skill in most cases. The activity centre model outperformed only the simple RW model when analysing data generated from a biased RW. Additionally, in our right whale case study, RW models received considerably more support in the data and predicted out-of-sample data with higher likelihood than did activity centre models.

Integrating SCR and movement models can address many questions important to ecology and conservation (McClintock et al., 2021). Here, we are interested in where the individuals in a population will be located in the near-term future. A SCR model addresses the question of how many individuals are in the population, while a hidden Markov model provides means to forecast each individual's location

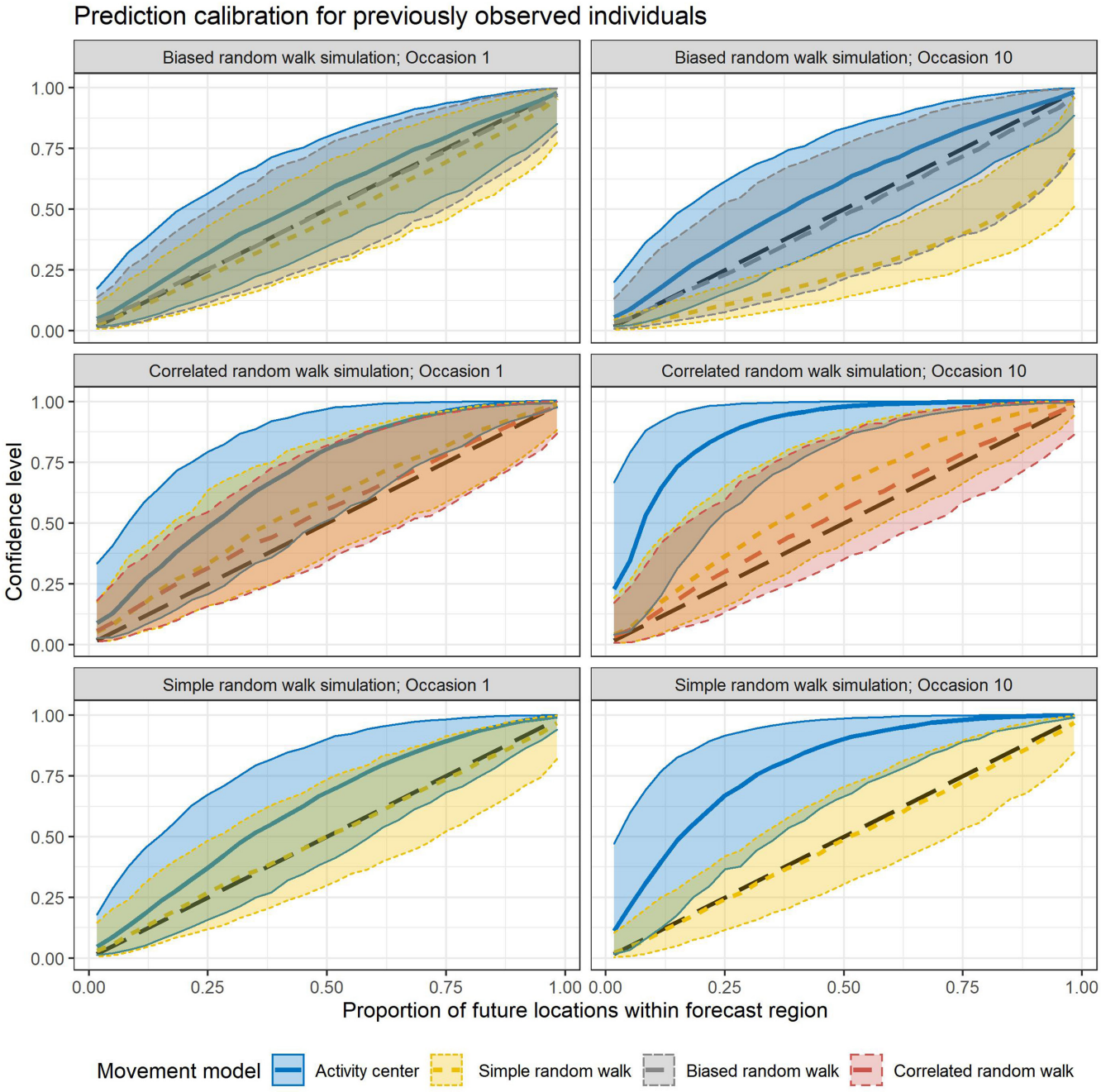

FIGURE 1 Calibration of individuals' forecasted locations one and 10 sampling occasions in the future (denoted by each panel's label) under spatial capture–recapture models with activity centre (blue), simple random walk (yellow), biased random walk (grey) and correlated random walk (red) movement models. We simulated 1000 datasets of 100 individuals moving according to simple, biased and correlated random walks (denoted by each panel's label) over 20 sampling occasions. We fit spatial capture–recapture models to the first 10 occasions and forecasted individuals' locations for the next 10 occasions. For individuals that were observed during the first 10 occasions, we calculated the proportion of their locations over the final 10 occasions that fell within forecast regions of varying confidence levels. Thick lines depict the mean of this proportion, and the bands include 95% of the proportions across the 1000 simulations. The black dashed line depicts perfect calibration. Models with calibration falling above the dashed line generate forecasts that include fewer true locations than expected and vice versa for models with calibration below the dashed line.

given their encounter histories and the estimated model parameters (Royle, Chandler, Gazenski, et al., 2013; Zucchini et al., 2016). Such an integrated model allows for the estimation and forecasting of individuals' locations, regardless of whether they have been previously observed or tagged.

This application could be especially useful in monitoring and mitigating threats to endangered species, like the right whale. Right whales are at risk of vessel strikes throughout their range, and many management and outreach activities are used to mitigate this threat (Crum et al., 2019; van der Hoop et al., 2014).

TABLE 2 North Atlantic right whale superpopulation ($\hat{N}$) and movement scale ($\hat{\sigma}_{move}$) in the southeastern United States between 1 December 2009 and 31 March 2010. Six spatial capture–recapture models were tested, two each with activity centre, simple random walk and correlated random walk movement models. One version of each model (AC, activity centre; SRW, simple random walk; and CRW, simplified correlated random walk) was formulated without environmental covariates included in the movement process (null), and the other version included quadratic effects of depth and sea surface temperature and a linear effect of wind speed (full). Models were fit to the full dataset and compared using AIC. Models were also fit to a reduced data set, which omitted eight sampling occasions, and compared based on the log-likelihood of the omitted data under forecasts generated by each model.

Model	AIC	ΔAIC	Forecast log-likelihood	$\hat{N}$	$\hat{\sigma}_{move}$ (km)
AC-null	14129.25	841.79	−953.98	239.5 (229.7–255.2)	35.0 (30.3–40.5)
AC-full	13683.53	396.07	−925.37	238.6 (229.2–253.6)	37.7 (31.6–44.9)
SRW-null	13593.79	306.33	−918.50	270.4 (252.6–296.4)	26.8 (24.5–29.3)
SRW-full	13306.88	19.42	−899.48	253.9 (240.3–274.6)	34.4 (30.8–38.4)
CRW-null	13617.53	330.07	−920.49	281.7 (261.0–311.5)	27.2 (17.8–36.5)
CRW-full	13287.46	0	−919.35	289.9 (267.9–320.9)	27.8 (20.7–37.4)

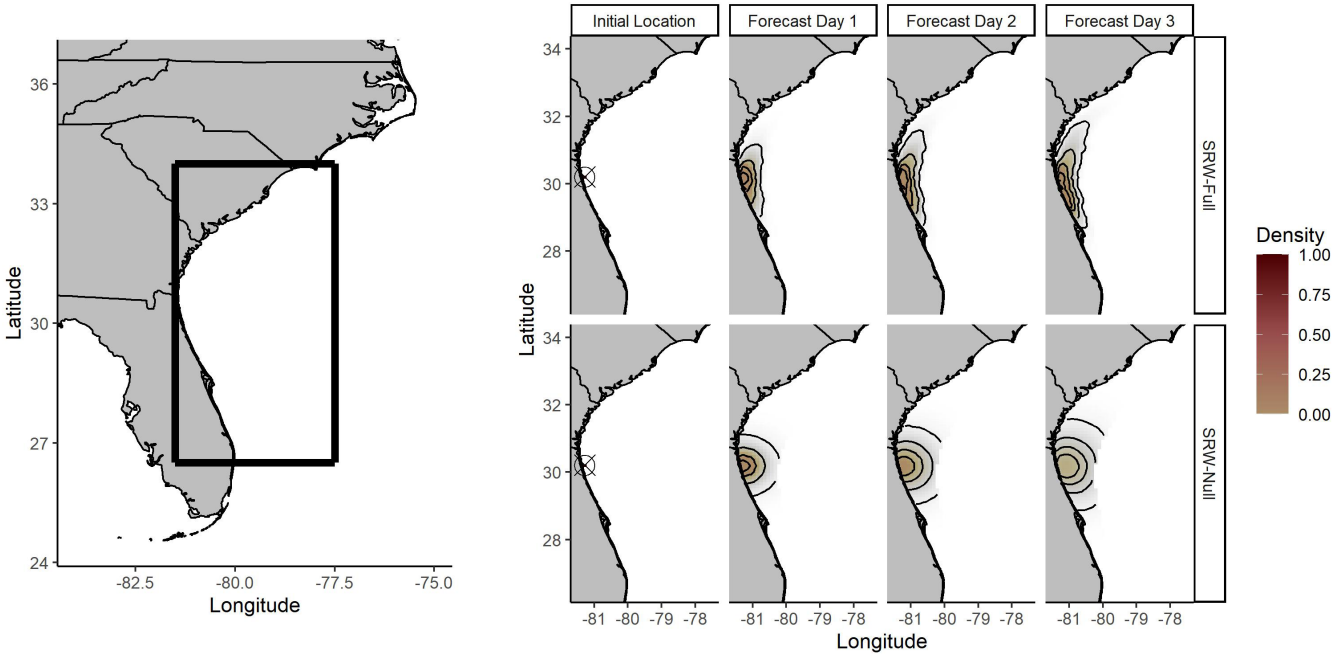

FIGURE 2 Example forecasts over 3 days following the detection of a right whale at the point with an X through it and circled in the left-most panels. From left to right, panels depict the initial location where the whale was observed, then forecasts for the whale's location 1, 2 and 3 days in the future. The forecasts on the top set of panels were generated from the simple random walk model with quadratic effects of depth and sea surface temperature and a linear effect of wind speed. The forecasts on the bottom set of panels were generated from the simple random walk model that did not include covariate effects. Contours represent the 25%, 50%, 75% and 95% prediction intervals.

Forecasting right whale movements could provide valuable information to plan and prioritize activities, such as dynamically enforced speed restrictions and broadcast notices to mariners. Additionally, forecasts could inform where monitoring effort should be allocated to observe individuals that have yet to be observed or track individuals of interest, such as reproductive females in the right whale population. However, when a species' movements are associated with temporally dynamic environmental covariates, forecasts of those covariates will be needed and will introduce an additional source of uncertainty (Payne et al., 2017). Movement forecasts should also be evaluated with out-of-sample data. In our right whale case study the correlated RW model with environmental covariates received the most support in the data according to AIC. However, that model estimated unreasonably high densities during one 10-day period in a few subregions at the edge of the study region. These subregions were not surveyed and had high and low sea surface temperatures, which resulted in the model estimating an unreasonable association between right whale movement and sea surface temperature (Appendix 2 in Figure S2). The likelihood of out-of-sample data under forecasts from each model exposed this artefact, as the simple RW forecasts clearly outperformed forecasts of the correlated RW.

Our simulation study demonstrated that integrated SCR movement models have the potential to produce properly calibrated forecasts of individuals' future movements based only on sparse SCR data. However, mismatches between the forecasting and simulating models led to poorly calibrated forecasts that performed increasingly poorly as the forecast extended farther into the future. Therefore, we advise testing multiple realistic movement models and comparing their performance in out-of-sample prediction before using a model's forecasts. In some cases, SCR data alone may not provide enough information to fit a realistic movement model. For instance, the correlated RW model estimated the γ and ω parameters, which describe the correlation of movement trajectories, with low precision in our simulation study (Appendix 1), and the correlated RW model fit to right whale data predicted right whale movements worse than the simple RW model. In such cases, additional information such as tagging data, which can increase the number of recaptures on consecutive sampling occasions, or individuals' directions and speeds of travel at the time of observation, which can be used to infer past and future locations, may need to be included in the analysis (Gardner et al., 2022; McClintock et al., 2021).

Forecasts are also affected by the uncertainty regarding individuals' current locations. This uncertainty increases as the amount of time since an individual was last observed increases, as the effectiveness and coverage of the detection process decrease, and as the scale of an individual's movement increases. Therefore, forecasts will be most informative for individuals that were observed recently, in systems that are subject to consistent and efficient sampling, and for species that move short distances. Hidden Markov models propagate the uncertainty regarding individuals' locations through their forecasts and account for the stochastic nature of the movement process. When none of the aforementioned conditions are met, the region in which an individual is forecasted to be located may be too large to be meaningful. In our right whale case study, forecasts may only be useful for a few days after an individual is observed, because individuals were estimated to move over 25 km per day on average. Still, females with calves, the demographic group of greatest importance to the population, are observed frequently in the Southeast (Gowan et al., 2019; Krzystan et al., 2018). Forecasts of their movements would likely be of greatest interest and could be information rich due to the frequency of their sightings.

In addition to describing an approach to forecast the movements of wildlife, we describe a maximum likelihood estimator for integrated SCR movement models. Most studies that integrated SCR and movement models have used a Bayesian approach, although Glennie et al. (2019) described a simple RW for activity centres, and Dupont et al. (2021) model the movements of tagged individuals with biased RWs, both using maximum likelihood estimation. We found that our models computed considerably faster when implemented with maximum likelihood estimation than with a Bayesian framework. However, maximum likelihood estimation may require a sparse matrix implementation when modelling movement at finer spatial scales, because the computation required for our implementation is proportional to the square of the number of subregions or states in the model (Zucchini et al., 2016). Additionally, a Bayesian approach may be easier and more flexible to implement, especially with software such as NIMBLE, which allows user-defined functions to be used in the model (de Valpine et al., 2017; Hostetter et al., 2022; Turek et al., 2021).

Much effort has been expended to project the distribution of wildlife populations in the long-term future (Payne et al., 2017), while only Randon et al. (2022) have developed near-term forecasting of wildlife movements. Integrated SCR movement models have only recently been developed and have many potential applications, including near-term movement forecasting. These models can forecast the movements of all individuals in a population of interest, whether they have been tagged, previously observed, or neither. In study systems with consistent and efficient SCR sampling, forecasts can provide valuable information to improve wildlife monitoring and threat mitigation activities.

AUTHOR CONTRIBUTIONS

Nathan J. Crum conceived the ideas and designed the methods with support from Timothy A. Gowan and Kandethody M. Ramachandran. Nathan J. Crum analysed the data with support from Timothy A. Gowan. Nathan J. Crum led the writing. All authors contributed to the review and revision of the manuscript.

ACKNOWLEDGEMENTS

We thank the aerial survey teams from Clearwater Marine Aquarium Research Institute, Florida Fish and Wildlife Conservation Commission and New England Aquarium for collecting the right whale data. We thank the North Atlantic Right Whale Consortium for curating and providing the photo ID data used in the right whale analysis. We thank Florent Bled, Brett McClintock and two anonymous reviewers for their helpful reviews of this manuscript. Funding for aerial surveys was provided by NOAA Fisheries, US Coast Guard, US Navy, US Army Corps of Engineers and Georgia Department of Natural Resources. Funding for the analysis was provided by NOAA Fisheries (NA16NMF4720319) and the Save the Manatee Trust Fund.

CONFLICT OF INTEREST STATEMENT

The authors declare no conflicts of interest.

PEER REVIEW

The peer review history for this article is available at https://www.webofscience.com/api/gateway/wos/peer-review/10.1111/2041-210X.14222.

DATA AVAILABILITY STATEMENT

The R package, scrrw, used for the simulation study is available via Zenodo https://doi.org/10.5281/zenodo.8338553 (nathancrum, 2023). The data and scripts used for the simulation study and the analysis of right whale aerial survey data are available via Dryad Digital Repository https://doi.org/10.5061/dryad.xpnvx0kn2 (Crum et al., 2023).

ORCID

Nathan J. Crum https://orcid.org/0000-0002-1253-7329
Timothy A. Gowan https://orcid.org/0000-0002-0082-1621

REFERENCES

Bischof, R., Milleret, C., Dupont, P., Chipperfield, J., Tourani, M., Ordiz, A., de Valpine, P., Turek, D., Royle, J. A., Gimenez, O., Flagstad, O., Akesson, M., Svensson, L., Broseth, H., & Kindberg, J. (2020). Estimating and forecasting spatial population dynamics of apex predators using transnational genetic monitoring. *Proceedings of the National Academy of Sciences of the United States of America*, *117*, 30531–30538. https://doi.org/10.1073/pnas.2011383117

Borchers, D. L., & Efford, M. G. (2008). Spatially explicit maximum likelihood methods for capture–recapture studies. *Biometrics*, *64*, 377–385. https://doi.org/10.1111/j.1541-0420.2007.00927.x

Buckland, S. T., Anderson, D. R., Burnham, K. P., Laake, J. L., Borchers, D. L., & Thomas, L. (2004). *Advanced distance sampling*. Oxford University Press.

Burnham, K. P., & Anderson, D. R. (2002). *Model selection and multimodel inferences: A practical information-theoretic approach*. Springer-Verlag.

Cagnacci, F., Boitani, L., Powell, R. A., & Boyce, M. S. (2010). Animal ecology meets GPS-based radiotelemetry: A perfect storm of opportunities and challenges. *Philosophical Transactions of the Royal Society B: Biological Sciences*, *365*, 2157–2162. https://doi.org/10.1098/rstb.2010.0107

Chandler, R. B., Crawford, D. A., Garrison, E. P., Miller, K. V., & Cherry, M. J. (2021). Modeling abundance, distribution, movement, and space use with camera and telemetry data. *Ecology*, *103*, e3583. https://doi.org/10.1002/ecy.3583

Crum, N., Gowan, T., Krzystan, A., & Martin, J. (2019). Quantifying risk of whale–vessel collisions across space, time, and management policies. *Ecosphere*, *10*, e2713. https://doi.org/10.1002/ecs2.2713

Crum, N., Gowan, T., & Ramachandran, K. (2023). Data from: Forecasting wildlife movement with spatial capture-recapture. *Dryad Digital Repository*. https://doi.org/10.5061/dryad.xpnvx0kn2

Crum, N. J., Neyman, L. C., & Gowan, T. A. (2021). Abundance estimation for line transect sampling: A comparison of distance sampling and spatial capture–recapture models. *PLoS ONE*, *16*, e0252231. https://doi.org/10.1371/journal.pone.0252231

De Valpine, P., Turek, D., Paciorek, C. J., Anderson-Bergman, C., Temple Lang, D., & Bodik, R. (2017). Programming with models: Writing statistical algorithms for general model structures with NIMBLE. *Journal of Computational and Graphical Statistics*, *26*, 403–417. https://doi.org/10.1080/10618600.2016.1172487

Dunn, P. K., & Smyth, G. K. (1996). Randomized quantile residuals. *Journal of Computational and Graphical Statistics*, *5*, 236–244. https://doi.org/10.2307/1390802

Dupont, G., Linden, D. W., & Sutherland, C. (2021). Improved inferences about landscape connectivity from spatial capture–recapture by integration of a movement model. *Ecology*, *103*, e3544. https://doi.org/10.1002/ecy.3544

Eddelbuettel, D., & Francois, R. (2011). Rcpp: Seamless R and C++ integration. *Journal of Statistical Software*, *40*, 1–18. https://doi.org/10.18637/jss.v040.i08

Eddelbuettel, D., & Sanderson, C. (2014). Rcpparmadillo: Accelerating r with high-performance C++ linear algebra. *Computational Statistics and Data Analysis*, *71*, 1054–1063. https://doi.org/10.1016/j.csda.2013.02.005

Efford, M. G., & Fewster, R. M. (2013). Estimating population size by spatially explicit capture–recapture. *Oikos*, *122*, 918–928. https://doi.org/10.1111/j.1600-0706.2012.20440.x

Efford, M. G., & Schofield, M. R. (2020). A spatial open-population capture–recapture model. *Biometrics*, *76*, 392–402. https://doi.org/10.1111/biom.13150

Gardner, B., McClintock, B. T., Converse, S. J., & Hostetter, N. J. (2022). Integrated animal movement and spatial capture–recapture models: Simulation, implementation, and inference. *Ecology*, *103*, e3771. https://doi.org/10.1002/ecy.3771

Gardner, B., Repucci, J., Lucherini, M., & Royle, J. A. (2010). Spatially explicit inference for open populations: Estimating demographic parameters from camera-trap studies. *Ecology*, *91*, 3376–3383. https://doi.org/10.1890/09-0804.1

Glennie, R., Borchers, D. L., Murchie, M., Harmsen, B. J., & Foster, R. J. (2019). Open population maximum likelihood spatial capture–recapture. *Biometrics*, *75*, 1345–1355. https://doi.org/10.1111/biom.13078

Gowan, T. A., Crum, N. J., & Roberts, J. J. (2021). An open spatial capture–recapture model for estimating density, movement, and population dynamics from line-transect surveys. *Ecology and Evolution*, *11*, 7354–7365. https://doi.org/10.1002/ece3.7566

Gowan, T. A., & Ortega-Ortiz, J. G. (2014). Wintering habitat model for the North Atlantic right whale (*Eubalaena glacialis*) in the southeastern United States. *PLoS ONE*, *9*, e95126. https://doi.org/10.1371/journal.pone.0095126

Gowan, T. A., Ortega-Ortiz, J. G., Hostetler, J. A., Hamilton, P. K., Knowlton, A. R., Jackson, K. A., George, R. C., Taylor, C. R., & Naessig, P. J. (2019). Temporal and demographic variation in partial migration of the North Atlantic right whale. *Scientific Reports*, *9*, 353. https://doi.org/10.1038/s41598-018-36723-3

Hazen, E. L., Palacios, D. M., Forney, K. A., Howell, E. A., Becker, E., Hoover, A. L., Irvine, L., DeAngelis, M., Bograd, S. J., Mate, B. R., & Bailey, H. (2017). WhaleWatch: A dynamic management tool for predicting blue whale density in the California current. *Journal of Applied Ecology*, *54*, 1415–1428. https://doi.org/10.1111/1365-2664.12820

Hooten, M. B., Johnson, D. S., McClintock, B. T., & Morales, J. M. (2017). *Animal movement: Statistical models for telemetry data*. CRC Press.

Hostetter, N. J., Regehr, E. V., Wilson, R. R., Royle, J. A., & Converse, S. J. (2022). Modeling spatiotemporal abundance and movement dynamics using an integrated spatial capture–recapture movement model. *Ecology*, *103*, e3772. https://doi.org/10.1002/ecy.3772

Krzystan, A. M., Gowan, T. A., Kendall, W. L., Martin, J., Ortega-Ortiz, J. G., Jackson, K., Knowlton, A. R., Naessig, P., Zani, M., Schulte, D. W., & Taylor, C. R. (2018). Characterizing residence patterns of North Atlantic right whales in the southeastern USA with a multistate open robust design model. *Endangered Species Research*, *36*, 279–295. https://doi.org/10.3354/esr00902

Matthiopoulos, J., Fieberg, J., Aarts, G., Beyer, H. L., Morales, J. M., & Haydon, D. T. (2015). Establishing the link between habitat selection and animal population dynamics. *Ecological Monographs*, *85*, 413–436. https://doi.org/10.1890/14-2244.1

McClintock, B. T., Abrahms, B., Chandler, R. B., Conn, P. B., Converse, S. J., Emmet, R. L., Gardner, B., Hostetter, N. J., & Johnson, D. S. (2021). An integrated path for spatial capture–recapture and animal movement modeling. *Ecology*, *103*, e3473. https://doi.org/10.1002/ecy.3473

Morales, J. M., Moorcroft, P. R., Matthiopoulos, J., Frair, J. L., Kie, J. G., Powell, R. A., Merrill, E. H., & Haydon, D. T. (2010). Building the bridge between animal movement and population dynamics. *Philosophical Transactions of the Royal Society B: Biological Sciences*, *365*, 2289–2301. https://doi.org/10.1098/rstb.2010.0082

Nathan, R., Getz, W. M., Revilla, E., Holyoak, M., Kadmon, R., Saltz, D., & Smouse, P. E. (2008). A movement ecology paradigm for unifying organismal movement research. *Proceedings of the National Academy of Sciences of the United States of America*, *105*, 19052–19059. https://doi.org/10.1073/pnas.0800375105

nathan-crum. (2023). nathan-crum/scrrw: scrrw (v1.0.0). Zenodo https://doi.org/10.5281/zenodo.8338553

Pace, R. M., Corkeron, P. J., & Kraus, S. D. (2017). State–space mark–recapture estimates reveal a recent decline in abundance of North Atlantic right whales. *Ecology and Evolution*, *7*, 8730–8741. https://doi.org/10.1002/ece3.3406

Patterson, T. A., Parton, A., Langrock, R., Blackwell, P. G., Thomas, L., & King, R. (2017). Statistical modelling of individual animal movement: An overview of key methods and a discussion of practical challenges. *AStA Advances in Statistical Analysis*, *101*, 399–438. https://doi.org/10.1007/s10182-017-0302-7

Payne, M. R., Hobday, A. J., MacKenzie, B. R., Tommasi, D., Dempsey, D. P., Fassler, S. M. M., Haynie, A. C., Ji, R., Liu, G., Lynch, P. D., Matei, D., Miesner, A. K., Mills, K. E., Strand, K. O., & Villarino, E. (2017). Lessons from the first generation of marine ecological forecast products. *Frontiers in Marine Science*, *4*, 289. https://doi.org/10.3389/fmars.2017.00289

R Core Team. (2019). *R: A language and environment for statistical computing*. R Foundation for Statistical Computing. https://www.R-project.org/

Randon, M., Dowd, M., & Joy, R. (2022). A real-time data assimilative forecasting system for animal tracking. *Ecology*, *103*, e3718. https://doi.org/10.1002/ecy.3718

Royle, J. A., Chandler, R. B., Gazenski, K. D., & Graves, T. A. (2013). Spatial capture–recapture models for jointly estimating population density and landscape connectivity. *Ecology*, *94*, 287–294. https://doi.org/10.1890/12-0413.1

Royle, J. A., Chandler, R. B., Sun, C. S., & Fuller, A. K. (2013). Integrating resource selection information with spatial capture–recapture. *Methods in Ecology and Evolution*, *4*, 520–530. https://doi.org/10.1111/2041-210X.12039

Royle, J. A., Sollman, R., Gardner, B., & Chandler, R. B. (2013). *Spatial Capture-Recapture*. Elsevier.

Runge, C. A., Martin, T. G., Possingham, H. P., Willis, S. G., & Fuller, R. A. (2014). Conserving mobile species. *Frontiers in Ecology and the Environment*, *12*, 395–402. https://doi.org/10.1890/130237

Turek, D., Milleret, C., Ergon, T., Broseth, H., Dupont, P., Bischof, R., & de Valpine, P. (2021). Efficient estimation of large-scale spatial capture–recapture models. *Ecosphere*, *12*, e0385. https://doi.org/10.1002/ecs2.3385

van der Hoop, J. M., Vanderlaan, A. S. M., Cole, T. V. N., Henry, A. G., Hall, L., Mase-Guthrie, B., Wimmer, T., & Moore, M. J. (2014). Vessel strikes to large whales before and after the 2008 ship strike rule. *Conservation Letters*, *8*, 24–32. https://doi.org/10.1111/conl.12105

Zucchini, W., MacDonald, I. L., & Langrock, R. (2016). *Hidden Markov models for time series: An Introduction using R* (2nd ed.). CRC Press.

SUPPORTING INFORMATION

Additional supporting information can be found online in the Supporting Information section at the end of this article.

Appendix 1. Supplemental simulation study results.

Table S1. Parameter values used to simulate spatial capture–recapture datasets.

Table S2. Average number of individuals detected per simulation (n) with 95% confidence intervals in parentheses and the proportion of individuals detected once, twice, etc. over 10 sampling occasions.

Table S3. Properties of spatial capture–recapture abundance estimates.

Table S4. Properties of spatial capture–recapture movement scale, σ_{move}, estimates.

Table S5. Properties of spatial capture–recapture detection probability at zero distance from the detector, $g0$, estimates.

Table S6. Properties of spatial capture–recapture detection scale, σ_d, estimates.

Table S7. Properties of spatial capture–recapture random walk bias (ρ), persistence (γ), and turning angle (ω) estimates.

Table S8. Properties of spatial capture–recapture random walk bias, β, estimates.

Figure S1. One individual's simple random walk across the simulation state space during 10 sampling occasions.

Figure S2. The movement distribution for the individual from Figure 1 between the first and second sampling occasions.

Figure S3. Ratios of the likelihoods of individuals' future locations under spatial capture–recapture models with activity centre and random walk movement models.

Figure S4. Calibration of individuals' forecasted locations over 10 future sampling occasions (denoted by each panel's label) under spatial capture–recapture models with activity centre (red) and random walk (blue) movement models.

Figure S5. One individual's biased random walk across the simulation state space during 10 sampling occasions.

Figure S6. The movement distribution for the individual from Figure 6 between the first and second sampling occasions.

Figure S7. Ratios of the likelihoods of individuals' future locations under spatial capture–recapture models with activity centre and biased random walk movement models (top) and random walk and biased random walk movement models (bottom).

Figure S8. Calibration of individuals' forecasted locations over 10 future sampling occasions (denoted by each panel's label) under spatial capture–recapture models with activity centre (red), random walk (green), and biased random walk (blue) movement models.

Figure S9. One individual's correlated random walk across the simulation state space during 10 sampling occasions.

Figure S10. The movement distribution for the individual from Figure 9 between the second and third sampling occasions.

Figure S11. Ratios of the likelihoods of individuals' future locations under spatial capture–recapture models with activity centre and correlated random walk movement models (top) and random walk and correlated random walk movement models (bottom).

Figure S12. Calibration of individuals' forecasted locations over 10 future sampling occasions (denoted by each panel's label) under spatial capture–recapture models with activity centre (red), random walk (green), and correlated random walk (blue) movement models.

Figure S13. Ratios of the likelihoods of individuals' future locations under spatial capture–recapture models with activity centre and simple random walk movement models.

Figure S14. Calibration of individuals' forecasted locations over 10 future sampling occasions (denoted by each panel's label) under spatial capture–recapture models with activity centre and simple random walk movement models.

Figure S15. Ratios of the likelihoods of individuals' future locations under spatial capture–recapture models with activity centre and simple random walk movement models.

Figure S16. Calibration of individuals' forecasted locations over 10 future sampling occasions (denoted by each panel's label) under spatial capture–recapture models with activity centre and simple random walk movement models.

Figure S17. Ratios of the likelihoods of individuals' future locations under spatial capture–recapture models with activity centre and simple random walk movement models.

Figure S18. Calibration of individuals' forecasted locations over 10 future sampling occasions (denoted by each panel's label) under spatial capture–recapture models with activity centre and simple random walk movement models.

Figure S19. Ratios of the likelihoods of individuals' future locations under spatial capture–recapture models with activity centre and simple random walk movement models.

Figure S20. Calibration of individuals' forecasted locations over 10 future sampling occasions (denoted by each panel's label) under spatial capture–recapture models with activity centre and simple random walk movement models.

Appendix 2. Supplemental north Atlantic right whale results.

Figure S1. Average expected (left) and realized (right) density of North Atlantic right whales off the Atlantic coast of Florida, Georgia, and South Carolina between 1 December 2009 and 31 March 2010.

Figure S2. Associations between North Atlantic right whale density and movement and depth (left), sea surface temperature (middle), and wind speed (right).

Figure S3. Estimated immigration, τ, (top) and persistence, φ, (bottom) rates and 95% confidence intervals for North Atlantic right whales in the southeastern United States from 1 December 2009 to 31 March 2010.

Figure S4. Estimated detection probability for a North Atlantic right whale given its distance from the closest aerial survey trackline.

How to cite this article: Crum, N. J., Gowan, T. A., & Ramachandran, K. M. (2023). Forecasting wildlife movement with spatial capture–recapture. *Methods in Ecology and Evolution*, *14*, 2844–2855. https://doi.org/10.1111/2041-210X.14222